



**HAL**  
open science

# LPV Static Output Feedback for Constrained Direct Tilt Control of Narrow Tilting Vehicles

Tran Anh-Tu Nguyen, Philippe Chevrel, Fabien Claveau

► **To cite this version:**

Tran Anh-Tu Nguyen, Philippe Chevrel, Fabien Claveau. LPV Static Output Feedback for Constrained Direct Tilt Control of Narrow Tilting Vehicles. *IEEE Transactions on Control Systems Technology*, 2018, 28 (2), pp.661-670. 10.1109/TCST.2018.2882345 . hal-01980168

**HAL Id: hal-01980168**

**<https://hal.science/hal-01980168v1>**

Submitted on 29 Apr 2022

**HAL** is a multi-disciplinary open access archive for the deposit and dissemination of scientific research documents, whether they are published or not. The documents may come from teaching and research institutions in France or abroad, or from public or private research centers.

L'archive ouverte pluridisciplinaire **HAL**, est destinée au dépôt et à la diffusion de documents scientifiques de niveau recherche, publiés ou non, émanant des établissements d'enseignement et de recherche français ou étrangers, des laboratoires publics ou privés.

# LPV Static Output Feedback for Constrained Direct Tilt Control of Narrow Tilting Vehicles

Anh-Tu Nguyen\*, *Member, IEEE*, Philippe Chevrel, Fabien Claveau

**Abstract**—This paper presents a new direct tilt control (DTC) design to improve the lateral stability and the driving comfort of narrow tilting vehicles. To this end, a conceptual model is constructed from the vehicle dynamics, a simplified model of the driving environment, and the vehicle perceived acceleration. This latter is considered as the main performance variable of the related  $\mathcal{H}_2$  control problem. The conceptual model is then represented in a polytopic linear parameter varying (LPV) form for control purposes. To avoid the use of costly vehicle sensors while favoring the simplest control structure for real-time implementation, a new LPV static output feedback (SOF) control method is proposed. Thanks to Lyapunov stability arguments, physical constraints on both system states and DTC actuator are *explicitly* considered in the design procedure to improve the safety and the comfort of passengers. Moreover, a parameter-dependent Lyapunov function is exploited for theoretical developments. In this way, the *finite* bounds on vehicle speed and acceleration are effectively taken into account in the control design to reduce the conservatism. The  $\mathcal{H}_2$  control design is recast as an LMI-based optimization which can be easily solved with numerical solvers. The resulting robust DTC controller is evaluated with realistic driving scenarios.

**Index Terms**—Narrow tilting vehicles, direct tilt control, static output feedback control, LPV control, vehicle dynamics, linear matrix inequality (LMI).

## I. INTRODUCTION

Narrow tilting vehicles (NTVs) have been increasingly studied as a promising solution to traffic congestion, pollution, and parking issues in urban areas [1]–[5]. Moreover, the reduced dimensions of NTVs also result in their high fuel efficiency [3], [4]. Due to their special features, NTVs are characterized by a high center of gravity (c.g.) leading to the major issue on roll stability [6]–[8]. Indeed, to maintain the vehicle stability, NTVs should lean while cornering as motorcycles to compensate the effects of the centrifugal force. Hence, effective tilt control systems are *essential* elements in any narrow vehicle system design, which greatly improves the acceptability of NTVs with respect to standard vehicles [7]. Up to now, a few NTV prototypes have been developed in the automotive industry, *e.g.*, F-300 Life Jet by Mercedes-Benz (1997), Brink Dynamics by Carver (2003), SMERA by Lumeneo (2008), Land Glider by Nissan (2009), see [3], [9] for more details.

Two main types of control systems are available for vehicle tilting [7]: direct tilt control (DTC), and steering tilt control (STC). STC relies on a steering actuator to control the vehicle tilt in the same way as a moto rider [10]. This control strategy has some drawbacks: (i) it is not suitable at low speeds, nor on slippery roads [3], (ii) it may require a large countersteering to tilt the vehicle which leads to a significant trajectory deviation and ride discomfort [10]. Using a dedicated tilt actuator, DTC strategy can directly control the vehicle roll. Then, DTC could be used to address the major drawbacks of STC. However, the main drawback of DTC consists in its energy consumption and discomfort at the beginning of curve taking [6]. It has been shown that the integrated approach, *i.e.*, the combination of STC and DTC, can lead to the best control performance [3], [11],

[12]. Unfortunately, this solution requires both a tilt actuator and a steer-by-wire system, which increases the cost of NTVs [10].

This work is the continuity of our collaboration with Lumeneo company in developing control strategies for the SMERA vehicle [6], [9]. This four-wheeled NTV has two seats in tandem and an DTC actuator for tilt control, see Fig. 1. As in our previous studies [6], a direct regulation/minimization of the perceived acceleration will be considered for the control design. This allows avoiding both the online computational complexity and the residual tilt torque, thus saving the energy consumption. The latter is caused by approximation errors of the tilt angle reference in tracking control approaches largely discussed in the literature, see [1]–[3], [5], [8], [11], [13] and references therein. Note that most of DTC methods have considered a *constant* vehicle speed to ease the design task, see [6], [10] for short surveys. However, the corresponding linear controllers cannot provide a satisfactory closed-loop performance under various driving circumstances [14]. Moreover, these methods are usually based on a state feedback control scheme which requires *full* vehicle sensor information for real-time implementation. This paper presents a systematic DTC method which can effectively address the above technical and practical control issues. The main contributions can be summarized as follows.

- Using an SOF control scheme, the proposed DTC controller is easily realized from engineering viewpoint without needing an important vehicle sensor to measure the lateral speed. Differently from [6], the new control method does not require any online estimation of the vehicle states which can lead to online computational burden, approximation errors, and especially an algebraic loop for real-time implementation. Moreover, similar to [6], the new method can be easily adapted to STC and integrated control approaches.
- LPV paradigm has been demonstrated as an effective tool for modeling and control in a variety of engineering applications, see [15]–[17] and related references. Here, the *time-varying* nature of the vehicle speed is tackled with a novel LPV control framework. Especially, the *finite* bounds on both vehicle speed and acceleration are *explicitly* considered in the  $\mathcal{H}_2$  control via a parameter-dependent Lyapunov function to reduce the design conservatism.
- The new DTC method can *explicitly* take into account the physical constraints on both the tilt torque and the system states in the  $\mathcal{H}_2$  control procedure to improve not only the energy consumption of DTC actuator but also the safety and the comfort of passengers. This major issue for lateral control of NTVs has not been well addressed in the open literature [8]. The closed-loop performance of the LPV vehicle system is theoretically proved using Lyapunov stability theory, which is not the case of most existing methods [6]. In particular, the design conditions are formulated as an LMI optimization which can be effectively solved with numerical solvers [18]. Note that LMI-based  $\mathcal{H}_2$  static output control for LPV systems still remains an open research topic [19]. The proposed theoretical results go beyond the scope of the considered application and can be applied to a larger class of LPV systems.

The paper is organized as follows. Section II presents the nonlinear model of NTVs used for simulation purposes and formulates the control goals. In Section III, we define an LPV standard model of NTVs used for lateral control purposes. Section IV presents a new robust SOF method allowing to achieve several control specifications

A.-T. Nguyen is with the LAMIH laboratory UMR CNRS 8201, Université Polytechnique Hauts-de-France, Valenciennes, France.

P. Chevrel and F. Claveau are with the IMT Atlantique, UBL, and the LS2N laboratory UMR CNRS 6004, Nantes, France. This work was done when A.-T. Nguyen was with the LS2N laboratory UMR CNRS 6004.

\*Corresponding author. E-mail: nguyen.trananhthu@gmail.com.

of NTVs. The effectiveness of the new DTC method is demonstrated in Section V. Conclusions are given in Section VI.

*Notation.*  $\Omega_N$  denotes the number set  $\{1, 2, \dots, N\}$ .  $I$  denotes the identity matrix of appropriate dimension. For a matrix  $X$ ,  $X^\top$  indicates its transpose, and  $X_{(i)}$  denotes its  $i$ th row. For any square matrix  $X$ ,  $X > 0$  indicates a symmetric positive definite matrix, and  $\text{He } X = X + X^\top$ .  $\text{diag}(\cdot)$  denotes a block diagonal matrix formed by the blocks given in the parenthesis. The  $i$ th element of a vector  $\mathbf{u}$  is denoted by  $\mathbf{u}_i$ , and  $\star$  stands for matrix blocks deduced by symmetry.  $\text{co}\{\mathcal{S}\}$  denotes the convex hull of the set  $\mathcal{S}$ . The time argument is dropped when convenient.



Fig. 1. Photo of the SMERA vehicle.

## II. VEHICLE MODELING AND PROBLEM DEFINITION

Several models of NTVs have been proposed for both simulation and control purposes, see for instance [7], [9], [12], [20], [21]. This section presents the nonlinear model of the SMERA vehicle used for our simulation study. Then, the related control problem is formulated. The vehicle nomenclature is given in Table I.

### A. Nonlinear Model of Narrow Commuter Vehicles

Fig. 2 depicts the four degrees of freedom (DOF) of the SMERA vehicle: the longitudinal and lateral positions  $(x, y)$  of the vehicle, the tilt angle  $\theta$ , and the yaw angle  $\psi$ . The corresponding dynamics model was developed in collaboration with Lumeneo company by inspiring from two nonlinear vehicle models. The first one focusses on the dynamics of the vehicle lateral position  $y$ , the tilt angle  $\theta$ , and the vehicle yaw  $\psi$  while considering a constant vehicle speed [7]. The second bicycle model represents both lateral and longitudinal dynamics [22]. Then, the SMERA dynamics is described by

$$\begin{aligned} m\dot{v}_x &= \mathcal{F}_{sf} \sin(\beta - \delta) + \mathcal{F}_{lf} \cos(\beta - \delta) + \mathcal{F}_{sr} \sin \beta \\ &\quad + \mathcal{F}_{lr} \cos \beta - \mathcal{F}_\theta \sin \beta \\ m v_x \dot{\beta} &= \mathcal{F}_{sf} \cos(\beta - \delta) - \mathcal{F}_{lf} \sin(\beta - \delta) + \mathcal{F}_{sr} \cos \beta \\ &\quad - \mathcal{F}_{lr} \sin \beta - m v_x \dot{\psi} - \mathcal{F}_\theta \cos \beta \\ I_z \dot{\psi} &= l_f (\mathcal{F}_{sf} \cos \delta + \mathcal{F}_{lf} \sin \delta) - l_r \mathcal{F}_{sr} \\ I_x \dot{\theta} &= m g h \sin \theta - m h^2 \dot{\theta}^2 \cos \theta \sin \theta - m h^2 \ddot{\theta} \sin^2 \theta \\ &\quad - (\mathcal{F}_{sf} \cos \delta + \mathcal{F}_{lf} \sin \delta + \mathcal{F}_{sr}) h \cos \theta + M_t \end{aligned} \quad (1)$$

where  $\mathcal{F}_\theta = m(h\ddot{\theta} \cos \theta - h\dot{\theta}^2 \sin \theta)$ ,  $\mathcal{I}_x = I_x + m h^2 \sin^2 \theta$  and  $v_y = v_x \sin \beta$ . The nonlinear lateral tire forces are modeled as

$$\mathcal{F}_{si} = F_{si}(\alpha_i) + 2\lambda_i \theta \quad (2)$$

for  $i \in \{f, r\}$ . The nonlinear forces  $F_{si}(\alpha_i)$  in (2) are modeled following the well-known Pacejka's magic formula [23]:

$$F_{si}(\alpha_i) = \mathcal{D}_i \sin(\mathcal{C}_i \arctan[(1 - \mathcal{E}_i) \mathcal{B}_i \alpha_i + \mathcal{E}_i \arctan(\mathcal{B}_i \alpha_i)])$$

where  $\mathcal{B}_i$ ,  $\mathcal{C}_i$ ,  $\mathcal{D}_i$  and  $\mathcal{E}_i$ , for  $i \in \{f, r\}$ , are the Pacejka parameters. The sideslip angles of the front/rear tires are given as follows [22]:

$$\begin{aligned} \alpha_f &= \delta - \arctan\left(\frac{v_x \sin \beta + l_f \dot{\psi}}{v_x \cos \beta}\right), \\ \alpha_r &= -\arctan\left(\frac{v_x \sin \beta - l_r \dot{\psi}}{v_x \cos \beta}\right). \end{aligned}$$

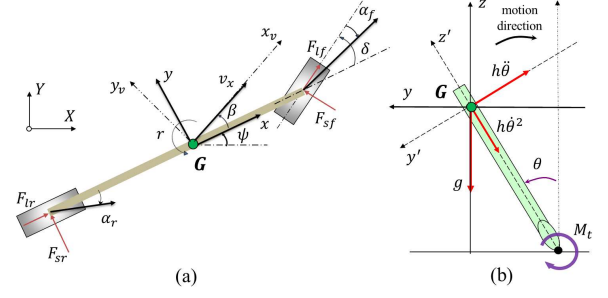


Fig. 2. Four degrees of freedom of SMERA: (a) top view; (b) rear view.

TABLE I  
VEHICLE NOMENCLATURE

Symbol	Description
$v_x$	Vehicle longitudinal speed
$v_y$	Vehicle lateral speed
$\beta$	Sideslip angle
$\psi$	Vehicle yaw angle
$\theta$	Vehicle tilt angle
$\delta$	Vehicle steering angle
$\mathcal{F}_{lf}/\mathcal{F}_{lr}$	Front/rear longitudinal force
$\mathcal{F}_{sf}/\mathcal{F}_{sr}$	Front/rear lateral force
$l_f/l_r$	Distance from c.g. $\mathbf{G}$ to front/rear wheels
$I_z/I_x$	Tilting/yaw moment of inertia of vehicle
$\mathcal{C}_f/\mathcal{C}_r$	Front/rear cornering stiffness
$\lambda_f/\lambda_r$	Front/rear camber stiffness
$\alpha_f/\alpha_r$	Front/rear tire sideslip angle
$g$	Gravitational constant
$h$	Height of c.g. $\mathbf{G}$ from ground
$m$	Mass of vehicle
$M_t$	Tilt torque from DTC actuator

### B. Available Sensors for Real-Time Control Implementation

As most of NTVs, SMERA is equipped with a tilt angle sensor and an inertial measurement unit (IMU), which provide the measurements of the vehicle states  $\theta$ ,  $\dot{\theta}$  and  $\dot{\psi}$ . An odometer is used to measure the vehicle speed  $v_x$  whereas the steering angle  $\delta$  and its derivative  $\dot{\delta}$  are obtained from an optical encoder. The IMU provides also the lateral acceleration  $a_{\text{per}}$  at the gravity center  $\mathbf{G}$ , defined as follows [7]:

$$a_{\text{per}} = (\dot{v}_y + v_x \dot{\psi}) \cos \theta + h \ddot{\theta} - g \sin \theta \quad (3)$$

The acceleration  $a_{\text{per}}$  plays a crucial role in the study of lateral stability of NTVs, and the comfort of passengers [6]–[8].

The sideslip angle  $\beta$  and the lateral speed  $v_y$  can be measured by a CORREVIT sensor. Unfortunately, due to the excessive cost of this optical sensor (about 15k€ per unit), the measurements of  $\beta$  and  $v_y$  are *unavailable* for control implementation [24]. This paper presents a systematic method for multiobjective lateral control of NTVs modeled by (1) which can handle this major practical issue.

### C. Problem Statement and Control Goals

Automatic DTC controllers aim to guarantee the lateral stability of NTVs, *i.e.*, to regulate the perceived acceleration  $a_{\text{per}}$  around zero during cornering [3]. Here, the following specifications are required for DTC control design.

- DTC controllers should be *easily* computed and implemented with only available vehicle sensors. The closed-loop control performance and robustness can be demonstrated using Lyapunov stability arguments.
- The integral of the perceived acceleration  $a_{\text{per}}$ , denoted by  $a_{\text{per}}^{\mathcal{T}}$ , should be *directly* regulated and minimized to: (i) avoid static errors during long curves, (ii) improve the comfort of passengers and the energy consumption [6].
- The constraints on both the system states and the tilt actuator should be *explicitly* taken into account in the control design to improve both the safety and the comfort of passengers.

To meet these specifications, we propose in Section IV a new LPV-based SOF control method in multiobjective setting.

### III. STANDARD MODEL FORMULATION FOR $\mathcal{H}_2$ CONTROL

Based on an  $\mathcal{H}_2$  control scheme, the proposed DTC method makes use of a standard model  $\Sigma$  composed of three generic elements: plant model  $\Sigma_p$ , environment model  $\Sigma_w$ , and model of regulated signals  $\Sigma_e$ , see Fig. 3. Next, these three elements are first defined in the similar way as in [6]. Then, we construct the corresponding control-based LPV standard model.

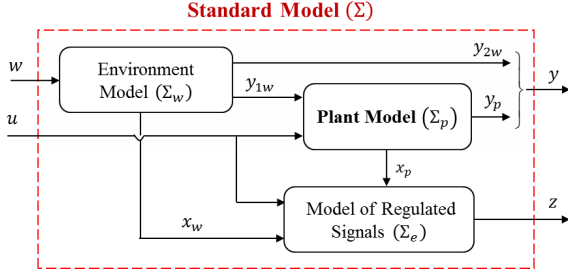


Fig. 3. Structure of the standard model  $\Sigma$  used for  $\mathcal{H}_2$  control design.

#### A. Vehicle Plant Model

For lateral control purposes, a 3 DOF vehicle model is derived from (1). To this end, the following usual assumptions are considered [7]. (i) The longitudinal dynamics is neglected. (ii) The lateral tire forces are proportional to the slip angles of each axle. (iii) The vehicle angles are small. It is important to note that these assumptions are relevant for normal driving conditions in urban areas which are the control focus of this paper. Then, the lateral dynamics of NTVs can be modeled as follows [8]:

$$\Sigma_p : \dot{\mathbf{x}}_p = A_p \mathbf{x}_p + B_p u + B_\delta \delta \quad (4)$$

where  $\mathbf{x}_p = [v_y \ \dot{\psi} \ \theta \ \dot{\theta}]^\top$  is the vehicle state vector, and the control input is the tilt torque from the DTC actuator  $\mathbf{u} = M_t$ . The system matrices of (4) are given by

$$A_p = \begin{bmatrix} a_{11} & a_{12} & a_{13} & 0 \\ a_{21} & a_{22} & a_{23} & 0 \\ 0 & 0 & 0 & 1 \\ a_{41} & a_{42} & a_{43} & 0 \end{bmatrix}, \quad B_{pu} = \begin{bmatrix} -\frac{h}{I_x} \\ 0 \\ 0 \\ \frac{1}{I_x} \end{bmatrix},$$

$$B_\delta = \begin{bmatrix} 2C_f \left( \frac{1}{m} + \frac{h^2}{I_x} \right) & \frac{2l_f C_f}{I_z} & 0 & -\frac{2hC_f}{I_x} \end{bmatrix}^\top,$$

where

$$a_{11} = -\frac{1}{v_x} \left( \frac{a}{m} + \frac{h^2 a}{I_x} \right), \quad a_{12} = -\frac{1}{v_x} \left( \frac{b}{m} + \frac{h^2 b}{I_x} \right) - v_x,$$

$$a_{13} = 2(\lambda_f + \lambda_r) \left( \frac{1}{m} + \frac{h^2}{I_x} \right) - \frac{mgh^2}{I_x}, \quad a_{21} = -\frac{b}{I_z v_x},$$

$$a_{22} = \frac{-2(l_r^2 C_r + l_f^2 C_f)}{I_x v_x}, \quad a_{23} = \frac{2(\lambda_f l_f - \lambda_r l_r)}{I_z},$$

$$a_{41} = \frac{ha}{I_x v_x}, \quad a_{42} = \frac{hb}{I_x v_x}, \quad a_{43} = \frac{mgh - 2h(\lambda_f + \lambda_r)}{I_x},$$

$$a = 2(C_r + C_f), \quad b = 2(C_f l_f - C_r l_r).$$

The output equation of system (4) is given by

$$\mathbf{y}_p = \begin{bmatrix} 0 & 1 & 0 & 0 \\ 0 & 0 & 1 & 0 \\ 0 & 0 & 0 & 1 \end{bmatrix} \mathbf{x}_p = C_p \mathbf{x}_p.$$

#### B. Environnement Model

The goal is to stabilize the lateral acceleration  $a_{\text{per}}$  under the variation of the steering actions. Hence, the environment model of  $\Sigma_p$  represents the *a priori* knowledge available on  $\delta$ . The following model is used for the curved trajectory prediction [6]:

$$\Sigma_w : \begin{cases} \dot{\mathbf{x}}_w = A_w \mathbf{x}_w + B_{1w} \mathbf{w} \\ \mathbf{y}_{1w} = C_{1w} \mathbf{x}_w, \quad \mathbf{y}_{2w} = C_{2w} \mathbf{x}_w \end{cases} \quad (5)$$

with  $\mathbf{x}_w = [\delta \ \dot{\delta}]^\top$ ,  $\mathbf{w}$  is an impulse signal and

$$A_w = \begin{bmatrix} 0 & 1 \\ -\alpha_1 \alpha_2 & -(\alpha_1 + \alpha_2) \end{bmatrix}, \quad C_{2w} = \begin{bmatrix} 1 & 0 \\ 0 & 1 \end{bmatrix},$$

$$B_{1w} = [0 \ 1]^\top, \quad C_{1w} = [1 \ 0],$$

where  $A_w$  is Hurwitz with  $\alpha_1 = 0.5$  and  $\alpha_2 = 1$ . The following remark is reported for the environment model  $\Sigma_w$ .

**Remark 1.** The environment model (5) represents the fact that the steering angle  $\delta$  is band limited and can be truncated in sequences of asymptotically convergent signals. Note that the time constant of  $\Sigma_w$  is about 2s which is reasonable for road curvature prediction in most real-world situations. This cannot be considered as a driver model since its dynamics does not depend on that of the vehicle. However, the consideration of such a *predictor* model in the control design offers a significant performance improvement. Especially, for the case of NTVs, the introduction of  $\dot{\delta}$  in the output  $\mathbf{y}_{2w}$  of  $\Sigma_w$  improves the *prediction* capacity of DTC controller with respect to curved trajectories to avoid an excessive tilt torque [6].

#### C. Model of Regulated Signals

As stated above, the integral of  $a_{\text{per}}$  should be directly controlled and minimized to improve the DTC performance. The model of the regulated signal  $a_{\text{per}}^{\mathcal{I}}$  is given by

$$\dot{a}_{\text{per}}^{\mathcal{I}} = a_{\text{per}} \quad (6)$$

From (3), model (6) can be represented in the following form by considering the small angles assumption:

$$\dot{a}_{\text{per}}^{\mathcal{I}} = a_{\text{per}} \approx \dot{v}_y + v_x \dot{\psi} + h\ddot{\theta} - g\theta$$

$$= (G_1 + G_2 A_p) \mathbf{x}_p + G_2 B_\delta \delta \quad (7)$$

where  $G_1 = [0 \ v_x \ -g \ 0]$  and  $G_2 = [1 \ 0 \ 0 \ h]$ . Moreover, following the guideline in [25], the performance vector  $\mathbf{z}$  associated to model (7) can be chosen as follows:

$$\mathbf{z} = \mathcal{W}_e(s) a_{\text{per}}, \quad \mathcal{W}_e(s) = \frac{\kappa s + M}{M \kappa s} \quad (8)$$

where the parameters  $M$  and  $\kappa$  are positive. The weighting function  $\mathcal{W}_e(s)$  is defined as above for two reasons. First, this guarantees that  $a_{\text{per}}$  should be less than  $M$  in magnitude at high frequencies. Second, we integrate an integral action and require a response time better than about  $\kappa$ .

From (6), (7) and (8), the model  $\Sigma_e$  can be represented as

$$\Sigma_e : \begin{cases} \dot{\mathbf{x}}_e = A_e \mathbf{x}_e + B_{ex} \mathbf{x}_p + B_{ew} \mathbf{x}_w \\ \mathbf{z} = D_{ex} \mathbf{x}_p + D_e \mathbf{x}_e + D_{ew} \mathbf{x}_w, \quad \mathbf{y}_e = C_e \mathbf{x}_e \end{cases} \quad (9)$$

where  $\mathbf{x}_e = a_{\text{per}}^{\mathcal{I}}$  and

$$A_e = 0, \quad B_{ex} = G_1 + G_2 A_p, \quad B_{ew} = [G_2 B_\delta \ 0],$$

$$D_{ex} = \frac{1}{M} B_{ex}, \quad D_e = \frac{1}{\kappa}, \quad D_{ew} = \frac{1}{M} B_{ew}, \quad C_e = 1.$$

#### D. Standard Model and Its Polytopic LPV Representation

From the definitions of  $\Sigma_p$  in (4),  $\Sigma_w$  in (5), and  $\Sigma_e$  in (9), the corresponding standard model  $\Sigma(v_x)$ <sup>1</sup> for  $\mathcal{H}_2$  control of the SMERA vehicle is constructed as follows:

$$\Sigma(v_x) : \begin{cases} \dot{\mathbf{x}} = A(v_x) \mathbf{x} + B_u \mathbf{u} + B_w \mathbf{w} \\ \mathbf{z} = C_z(v_x) \mathbf{x}, \quad \mathbf{y} = C_y \mathbf{x} \end{cases} \quad (10)$$

where  $\mathbf{x}^\top = [\mathbf{x}_p^\top \ \mathbf{x}_e^\top \ \mathbf{x}_w^\top]$ ,  $\mathbf{y}^\top = [\mathbf{y}_p^\top \ \mathbf{y}_e^\top \ \mathbf{y}_w^\top]$  and

$$A(v_x) = \begin{bmatrix} A_p & 0 & B_\delta C_{1w} \\ B_{ex} & A_e & B_{ew} \\ 0 & 0 & A_w \end{bmatrix}, \quad B_u = \begin{bmatrix} B_{pu} \\ 0 \\ 0 \end{bmatrix},$$

$$C_z^\top(v_x) = [D_{ex}^\top \ D_e^\top \ D_{ew}^\top], \quad B_w^\top = [0 \ 0 \ B_{1w}^\top],$$

$$C_y = \text{diag}(C_p, C_e, C_{2w}).$$

<sup>1</sup>The notation  $\Sigma(v_x)$  is simply to make clear that the system dynamics depends *explicitly* on the time-varying parameter  $v_x$ .

**Remark 2.** Note that the dynamics matrix and the performance matrix of the standard model  $\Sigma(v_x)$  depend *explicitly* on the time-varying speed which is measured and bounded

$$v_{\min} \leq v_x \leq v_{\max}, \quad v_{\min} = 2 \text{ [m/s]}, \quad v_{\max} = 18 \text{ [m/s]} \quad (11)$$

Different methods using different LPV representations, *e.g.*, linear fractional transformation (LFT) form, polytopic descriptor form, etc. [17], can be applied for the control design of LPV system (10). However, a polytopic LPV formulation has been chosen here since it leads to a simple characterization of the LPV controller for NTVs. As shown later, the proposed control solution is also of reasonable complexity for real-time implementation.

There are two *dependently* varying parameters involved in the dynamics of LPV system (10), *i.e.*,  $\omega_*(t) = \left[ v_x \quad \frac{1}{v_x} \right]^\top$ . These parameters form a convex hull  $\mathcal{P}_\omega$  with four vertices

$$\begin{aligned} \omega_{v1} &= \begin{bmatrix} v_{\min} & \frac{1}{v_{\min}} \end{bmatrix}^\top, & \omega_{v2} &= \begin{bmatrix} v_{\min} & \frac{1}{v_{\max}} \end{bmatrix}^\top, \\ \omega_{v3} &= \begin{bmatrix} v_{\max} & \frac{1}{v_{\max}} \end{bmatrix}^\top, & \omega_{v4} &= \begin{bmatrix} v_{\max} & \frac{1}{v_{\min}} \end{bmatrix}^\top. \end{aligned}$$

Observe in Fig. 4 that the parameter polytope  $\mathcal{P}_\omega$  with four vertices leads to design conservatism and numerical complexity. This is due to the fact that  $v_x$  and  $\frac{1}{v_x}$  are separately considered despite its strong dependency. Note that  $v_x$  and  $\frac{1}{v_x}$  only evolve on the curve  $\mathcal{C}_*$ , and the vertices  $\omega_{v2}$  and  $\omega_{v4}$  are *unreachable* for any value of  $v_x$ . Here, to take into account this strong dependency and to reduce significantly the numerical complexity of the control structure, we make use of the following variable change:

$$v_x = \frac{v_0 v_1}{v_1 + v_0 \omega} \Leftrightarrow \frac{1}{v_x} = \frac{1}{v_0} + \frac{1}{v_1} \omega \quad (12)$$

where the new parameter  $\omega$  used for gain scheduling satisfies

$$\omega_{\min} \leq \omega \leq \omega_{\max}, \quad \omega_{\min} = -1, \quad \omega_{\max} = 1 \quad (13)$$

The two constants  $v_0$  and  $v_1$  in (12) are given by

$$v_0 = \frac{2v_{\min}v_{\max}}{v_{\min} + v_{\max}}, \quad v_1 = \frac{2v_{\min}v_{\max}}{v_{\min} - v_{\max}}.$$

It is easy to verify that  $v_x = v_{\min}$  for  $\omega = \omega_{\min}$  and  $v_x = v_{\max}$  for  $\omega = \omega_{\max}$ . Hence,  $\omega$  can be used to describe the variation of  $v_x$  between its lower and upper bounds. Moreover, using the Taylor's approximation as in [26], the vehicle speed can be also approximated from the second expression in (12) by  $v_x \simeq v_0 \left( 1 - \frac{v_0}{v_1} \omega \right)$ . As a consequence, the parameter curve  $\mathcal{C}_*$  is approximated by the straight line  $\mathcal{C}$ , see Fig. 4. Remark that the expressions of both  $v_x$  and  $1/v_x$  are now *linearly* dependent on  $\omega$ . Substituting these expressions into (10), it can be easily observed that the corresponding standard model of the SMERA vehicle

$$\Sigma(\omega) : \begin{cases} \dot{\mathbf{x}} = A(\omega)\mathbf{x} + B_u \mathbf{u} + B_w \mathbf{w} \\ \mathbf{z} = C_z(\omega)\mathbf{x}, \quad \mathbf{y} = C_y \mathbf{x} \end{cases} \quad (14)$$

depends *linearly* on the new time-varying parameter  $\omega$ . Using the sector nonlinearity approach [27, Chapter 2],  $\Sigma(\omega)$  defined in (14) can be *exactly* represented in the polytopic LPV form

$$\Sigma(\omega) : \begin{cases} \dot{\mathbf{x}} = \sum_{i=1}^2 \eta_i(\omega)(A_i \mathbf{x} + B_i^u \mathbf{u} + B_i^w \mathbf{w}) \\ \mathbf{z} = \sum_{i=1}^2 \eta_i(\omega)C_i^z \mathbf{x}, \quad \mathbf{y} = C_y \mathbf{x} \end{cases} \quad (15)$$

where the membership functions (MFs), also called barycentric coordinates, and the state-space matrices are given by

$$\begin{aligned} \eta_1(\omega) &= \frac{1-\omega}{2}, & \eta_2(\omega) &= 1 - \eta_1(\omega), \\ A_1 &= A(\omega_{\min}), & B_1^u &= B_2^u = B_u, & B_1^w &= B_2^w = B_w, \\ A_2 &= A(\omega_{\max}), & C_1^z &= C_z(\omega_{\min}), & C_2^z &= C_z(\omega_{\max}). \end{aligned}$$

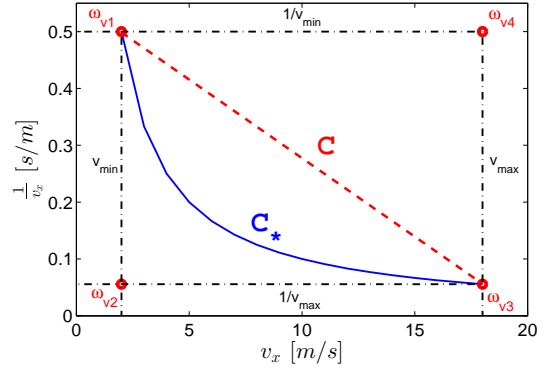


Fig. 4. Four-vertices polytope  $\mathcal{P}_\omega$  of  $\omega_*$ .

It is clear now that using the variable change (12) together with the above Taylor's approximation, the number of vertices is reduced from four to two. From the practical viewpoint, note that the induced approximation error is expected to be small over the whole system (10) since only a part of the element  $a_{12}$  of matrix  $A_p$  in (4) is affected by this approximation. This is also justified by experimental results on vehicle control presented in [26].

**Remark 3.** Besides the bounds on the vehicle speed (11), those of the vehicle acceleration  $a_x = \dot{v}_x$  are also given

$$a_{\min} \leq a_x \leq a_{\max}, \quad a_{\max} = -a_{\min} = 3.5 \text{ [m/s}^2\text{]} \quad (16)$$

These physical acceleration bounds allow to limit the theoretical kinematic centripetal acceleration of the vehicle [14]. From (12) and (16), it follows that

$$\frac{a_{\min}}{a_0} \leq \dot{\omega} \leq \frac{a_{\max}}{a_0}, \quad \text{with } a_0 = -\frac{v_0^2}{v_1}. \quad (17)$$

As proved later, an *explicit* consideration of the bounds on both vehicle speed and acceleration via (13) and (17) in the control design allows reducing further the design conservatism.

#### IV. LPV MULTIOBJECTIVE STATIC OUTPUT CONTROL

This section presents new conditions to design a multiobjective SOF controller that will be used for the SMERA vehicle.

##### A. Preliminaries

Let us consider LPV system (15) in the general form

$$\begin{aligned} \dot{\mathbf{x}} &= \sum_{i=1}^N \eta_i(\omega)(A_i \mathbf{x} + B_i^u \mathbf{u} + B_i^w \mathbf{w}) \\ \mathbf{z} &= \sum_{i=1}^N \eta_i(\omega)(C_i^z \mathbf{x} + D_i^z \mathbf{u}), \quad \mathbf{y} = C_y \mathbf{x} \end{aligned} \quad (18)$$

where  $\mathbf{x} \in \mathbb{R}^{n_x}$  is the state,  $\mathbf{u} \in \mathbb{R}^{n_u}$  is the control input,  $\mathbf{w} \in \mathbb{R}^{n_w}$  is the disturbance,  $\mathbf{z} \in \mathbb{R}^{n_z}$  is the performance output, and  $\mathbf{y} \in \mathbb{R}^{n_y}$  is the system output. The scheduling vector  $\omega \in \mathbb{R}^{n_\omega}$  is measured and assumed to be confined to a compact set  $\mathcal{P}_\omega \subset \mathbb{R}^{n_\omega}$ , defined by the following convex hull:

$$\mathcal{P}_\omega = \text{co} \{ \omega_{v1}, \omega_{v2}, \dots, \omega_{vN} \} \quad (19)$$

where the vertices  $\omega_{vi}$ ,  $i \in \Omega_N$ , are determined by all combinations of the upper and lower bounds  $\omega_{i \min}$  and  $\omega_{i \max}$  of individual scheduling parameters. The constant matrices  $A_i$ ,  $B_i^u$ ,  $B_i^w$ ,  $C_i^z$ ,  $C_y$ ,  $i \in \Omega_N$ , are of adequate dimensions. The MFs in (18) satisfy the property

$$\begin{aligned} \sum_{i=1}^N \eta_i(\omega) &= 1, & \sum_{i=1}^N \dot{\eta}_i(\omega) &= 0 \\ \eta_i(\omega) &\geq 0, & \phi_{i1} \leq \dot{\eta}_i(\omega) &\leq \phi_{i2} \end{aligned} \quad (20)$$

where  $\phi_{i1} \leq \phi_{i2}$  are *known* lower and upper bounds of  $\dot{\eta}_i(\omega)$ .

**Remark 4.** Given the bounds of  $\omega$  and its rate of variation  $\dot{\omega}$ , the values of  $\phi_{i1}$  and  $\phi_{i2}$ , for  $i \in \Omega_N$ , can be easily obtained, e.g., it follows from (13) and (17) that

$$\phi_{11} \leq \dot{\eta}_1(\omega) \leq \phi_{12}, \quad \phi_{21} \leq \dot{\eta}_2(\omega) \leq \phi_{22},$$

where

$$\phi_{11} = \frac{-a_{\max}}{2a_0}, \quad \phi_{12} = \frac{-a_{\min}}{2a_0}, \quad \phi_{21} = \frac{a_{\min}}{2a_0}, \quad \phi_{22} = \frac{a_{\max}}{2a_0}.$$

We consider the parameter-dependent SOF controller

$$\mathbf{u} = \sum_{i=1}^N \eta_i(\omega) K_i \mathbf{y} = K(\omega) \mathbf{y} \quad (21)$$

From (18) and (21), the closed-loop system is rewritten as

$$\Sigma_{cl}(\omega) : \begin{cases} \dot{\mathbf{x}} = \hat{A}(\omega) \mathbf{x} + B_w(\omega) \mathbf{w} \\ \mathbf{z} = \hat{C}_z(\omega) \mathbf{x} \end{cases} \quad (22)$$

where  $\hat{A}(\omega) = A(\omega) + B_u(\omega)K(\omega)C_y$ ,  $\hat{C}_z(\omega) = C_z(\omega) + D_z(\omega)K(\omega)C_y$ . This paper proposes a constructive solution for the following control problem.

**Problem 1.** Determine the parameter-dependent matrix gain  $K(\omega)$  such that the SOF controller (21) stabilizes LPV system (18) while minimizing the  $\mathcal{H}_2$  norm  $\|\Sigma_{cl}(\omega)\|_2$  of the closed-loop system (22) with  $\omega \in \mathcal{P}_\omega$ ,  $\forall t > 0$ , and the compact set  $\mathcal{P}_\omega$  is defined in (19).

Note that the  $\mathcal{H}_2$  control performance is considered to achieve a robust regulation of the lateral acceleration  $a_{\text{per}}$  under the variation of the steering actions. Hence, this allows improving the DTC performance of the SMERA vehicle during bend taking. For stability analysis and control design, we consider the following parameter-dependent Lyapunov function (PDLF):

$$V(\mathbf{x}) = \mathbf{x}^\top \left( \sum_{i=1}^N \eta_i(\omega) Q_i \right)^{-1} \mathbf{x} = \mathbf{x}^\top Q(\omega)^{-1} \mathbf{x} \quad (23)$$

where  $Q_i > 0$ , for  $\forall i \in \Omega_N$ . The following result is standard in the  $\mathcal{H}_2$  control framework, see for example [28].

**Lemma 1.** Consider LPV system  $\Sigma_{cl}(\omega)$  in (22) with  $\omega \in \mathcal{P}_\omega$ ,  $\forall t > 0$ . If there exist a positive definite matrix  $Q(\omega) \in \mathbb{R}^{n_x \times n_x}$ , a matrix  $Z(\omega) \in \mathbb{R}^{n_w \times n_w}$ , and a positive scalar  $\gamma$  such that

$$\begin{bmatrix} \text{He} \left( \hat{A}(\omega) Q(\omega) \right) - \dot{Q}(\omega) & \star \\ \hat{C}_z(\omega) Q(\omega) & -I \end{bmatrix} < 0 \quad (24)$$

$$\begin{bmatrix} Z(\omega) & \star \\ B_w(\omega) & Q(\omega) \end{bmatrix} > 0 \quad (25)$$

$$\text{trace}(Z(\omega)) < \gamma^2 \quad (26)$$

Then, it follows that  $\|\Sigma_{cl}(\omega)\|_2 < \gamma$  and the associate Lyapunov function of LPV system (22) is given in (23).

**Remark 5.** The design conditions in Lemma 1 depend *explicitly* on both  $\omega$  and  $\dot{\omega}$  (via the term  $\dot{Q}(\omega)$ ). Moreover, the control gain  $K(\omega)$  appears *nonlinearly* in the expressions of  $\hat{A}(\omega)$  and  $\hat{C}_z(\omega)$  in (22). Hence, it is not trivial to obtain an effective solution from such conditions. On the basis of Lemma 1, we propose hereafter new tractable conditions to design an SOF controller (21).

In the framework of polytopic systems, many control design conditions can be represented in the following form [29]:

$$\Upsilon(\omega) = \sum_{i=1}^N \sum_{j=1}^N \eta_i(\omega) \eta_j(\omega) \Upsilon_{ij} < 0 \quad (27)$$

where matrices  $\Upsilon_{ij}$  are *linearly* dependent on the decision variables and  $\omega \in \mathcal{P}_\omega$ . To convert the parameter-dependent condition (27) into a finite set of LMIs while avoiding excessive computational burden of parameter-gridding algorithms, the MFs have to be dropped out.

Without involving slack variables, the following lemma leads to a good tradeoff between numerical complexity and conservatism [30].

**Lemma 2.** Let  $\Upsilon_{ij}$ ,  $i, j \in \Omega_N$ , be symmetric matrices of appropriate dimensions, and  $\{\eta_i\}_{i \in \Omega_N}$  be a family of functions satisfying (20). Condition (27) holds if

$$\Upsilon_{ii} < 0, \quad \frac{2}{N-1} \Upsilon_{ii} + \Upsilon_{ij} + \Upsilon_{ji} < 0 \quad (28)$$

for  $i, j \in \Omega_N$ , and  $i < j$ .

Using slack variables, relaxation results with different degrees of design conservatism and/or computational complexity can be found in [29].

### B. LMI-Based $\mathcal{H}_2$ Static Output Feedback Control

The following theorem provides LMI-based conditions to design an  $\mathcal{H}_2$  SOF controller (21) for LPV system (18).

**Theorem 1.** Given an LPV system (18) with  $\omega \in \mathcal{P}_\omega$ ,  $\forall t > 0$ . If there exist symmetric positive definite matrices  $Q_i \in \mathbb{R}^{n_x \times n_x}$ , matrices  $M_i \in \mathbb{R}^{n_u \times n_u}$ ,  $X \in \mathbb{R}^{n_y \times n_y}$ ,  $Z_i \in \mathbb{R}^{n_w \times n_w}$ , for  $i \in \Omega_N$ , and positive scalars  $\epsilon$ ,  $\gamma$  satisfying the following optimization:

$$\text{minimize } \gamma^2$$

subject to

$$\begin{bmatrix} Z_i & \star \\ B_i^w & Q_i \end{bmatrix} > 0 \quad (29)$$

$$\text{trace}(Z_i) < \gamma^2 \quad (30)$$

$$\Phi_{ii}^{klm} < 0, \quad \frac{2}{N-1} \Phi_{ii}^{klm} + \Phi_{ij}^{klm} + \Phi_{ji}^{klm} < 0 \quad (31)$$

for  $i, j, k, l \in \Omega_N$ ,  $i < j$ ,  $k \neq l$ , and  $m \in \Omega_2$ . The quantity  $\Phi_{ij}^{klm}$  is defined as follows:

$$\Phi_{ij}^{klm} = \text{He} \begin{bmatrix} \Phi_{[11]ij}^{klm} & 0 & \epsilon B_i^u M_j \\ D_i^z M_j C_y + C_i^z Q_j & -I/2 & \epsilon D_i^z M_j \\ C_y Q_j - X C_y & 0 & -\epsilon X \end{bmatrix} \quad (32)$$

with  $\Phi_{[11]ij}^{klm} = A_i Q_j + B_i^u M_j C_y - \phi_{km}(Q_k - Q_l)/2$ . Then, the SOF controller (21) solves Problem 1. Moreover, the control feedback gains in (21) are given by

$$K_i = M_i X^{-1}, \quad i \in \Omega_N \quad (33)$$

*Proof.* Multiplying (29) by  $\eta_i(\omega) \geq 0$  and summing up for all  $i \in \Omega_N$ , we obtain (25). In the same fashion, (30) implies (26). Note from the definition of  $\Phi_{ij}^{klm}$  in (32) that if (31) holds, it follows that  $X + X^\top > 0$ . This guarantees the *nonsingularity* of  $X$ , thus the validity of the gain expression in (33).

Exploiting the constraint  $\sum_{i=1}^N \dot{\eta}_i(\omega) = 0$  in (20), it can be easily deduced that

$$\dot{Q}(\omega) = \dot{\eta}_l(\omega) Q_l + \sum_{\substack{k=1 \\ k \neq l}}^N \dot{\eta}_k(\omega) Q_k = \sum_{\substack{k=1 \\ k \neq l}}^N \dot{\eta}_k(\omega) (Q_k - Q_l) \quad (34)$$

For any  $\phi_{k1} \leq \dot{\eta}_k(\omega) \leq \phi_{k2}$ , we can rewrite

$$\dot{\eta}_k(\omega) = \chi_{k1}(\omega) \phi_{k1} + \chi_{k2}(\omega) \phi_{k2}, \quad k \in \Omega_N \quad (35)$$

where

$$\chi_{k1}(\omega) = \frac{\phi_{k2} - \dot{\eta}_k(\omega)}{\phi_{k2} - \phi_{k1}}, \quad \chi_{k2}(\omega) = \frac{\dot{\eta}_k(\omega) - \phi_{k1}}{\phi_{k2} - \phi_{k1}}.$$

Note that  $\chi_{kl}(\omega) \geq 0$ ,  $\sum_{l=1}^2 \chi_{kl}(\omega) = 1$ , for  $k \in \Omega_N$ . From (34) and (35),  $\dot{Q}(\omega)$  can be *exactly* represented as follows:

$$\dot{Q}(\omega) = \sum_{\substack{k=1 \\ k \neq l}}^N \sum_{m=1}^2 \chi_{km}(\omega) \phi_{km} (Q_k - Q_l) \quad (36)$$

Using expressions (32) and (36), condition (31) can be equivalently represented by (28), where

$$\Upsilon_{ij} = \text{He} \begin{bmatrix} \Upsilon_{[11]ij} & 0 & \epsilon B_i^u M_j \\ D_i^z M_j C_y + C_i^z Q_j & -I/2 & \epsilon D_i^z M_j \\ C_y Q_j - X C_y & 0 & -\epsilon X \end{bmatrix},$$

and  $\Upsilon_{[11]ij} = A_i Q_j + B_i^u M_j C_y - \dot{Q}(\omega)/2$ . By Lemma 2, condition (28) implies clearly that

$$\Upsilon(\omega) = \text{He} \begin{bmatrix} \Upsilon_{[11]}(\omega) & 0 & \epsilon B_u(\omega) M(\omega) \\ \Upsilon_{[21]}(\omega) & -I/2 & \epsilon D_z(\omega) M(\omega) \\ \Upsilon_{[31]}(\omega) & 0 & -\epsilon X \end{bmatrix} < 0 \quad (37)$$

where  $\Upsilon_{[11]}(\omega) = A(\omega)Q(\omega) + B_u(\omega)M(\omega)C_y - \dot{Q}(\omega)/2$ ,  $\Upsilon_{[21]}(\omega) = D_z(\omega)M(\omega)C_y + C_z(\omega)Q(\omega)$  and  $\Upsilon_{[31]}(\omega) = C_y Q(\omega) - X C_y$ . Pre- and postmultiplying (37) with  $\begin{bmatrix} I & 0 & B_u(\omega)M(\omega)X^{-1} \\ 0 & I & D_z(\omega)M(\omega)X^{-1} \end{bmatrix}$  and its transpose, we obtain (24) after some simple but tedious algebraic manipulations. By Lemma 1, the proof of Theorem 1 can be now concluded.  $\square$

**Remark 6.** The information on both  $\omega$  and  $\dot{\omega}$  is *explicitly* considered in the control design by exploiting the bounds  $\phi_{kl}$ , for  $k \in \Omega_N$ ,  $l \in \Omega_2$ , see Remark 4. This allows using the PDLF (23) to reduce the design conservatism. Indeed, if condition (31) is feasible for *arbitrarily* high variation of the MFs, *i.e.*,  $\phi_{k1} \rightarrow -\infty$  and  $\phi_{k2} \rightarrow +\infty$ ,  $\forall k \in \Omega_N$ , then the only possible solution is  $Q_1 \approx \dots \approx Q_N$  to minimize the effects of  $\phi_{km}(Q_k - Q_l)$  involved in (32). On the other hand, if one imposes that  $Q_i = Q$ , for  $\forall i \in \Omega_N$ , in (23), then the common quadratic Lyapunov function  $V(\mathbf{x}) = \mathbf{x}^\top Q^{-1} \mathbf{x}$  is recovered. This discussion shows that the result of Theorem 1 includes precisely that of quadratic approaches. A similar conclusion for the case of state-feedback control of affine LPV systems can be found in [28], [31].

### C. Constraints on Control Input and System States

It has been shown that even the NTV is at an equilibrium in a perfectly coordinated turn, *i.e.*, only a small amount of torque is required for small deviations, tilting the vehicle into a turn at high speeds may require excessive torque values [8]. Hence, to improve the energy consumption of the tilt actuator and also the ride qualities, the amplitude-limitation  $|\mathbf{u}(t)| \leq \bar{u}$ ,  $\forall t \geq 0$ , where  $\bar{u}$  is the actuator saturation level, should be imposed for control design. Moreover, as shown in [26] and in the sequel, many safety and comfort criteria can be mathematically translated into state constraints of the form

$$\mathbf{x} \in \mathcal{D}_x = \{ \mathbf{x} \in \mathbb{R}^{n_x} : |H_{(m)} \mathbf{x}| \leq 1, \quad m \in \Omega_q \} \quad (38)$$

where the given matrix  $H \in \mathbb{R}^{q \times n_x}$  characterizes the state domain  $\mathcal{D}_x$ . Hence, taking into account *explicitly* the state constraints (38) in the control design is crucial to improve both the safety and the comfort of passengers. Such design constraints can be represented in terms of matrix inequalities as shown in the following theorem.

**Theorem 2.** Given an LPV system (18) with  $\omega \in \mathcal{P}$ ,  $\forall t > 0$ , and  $|\mathbf{x}(0)| \leq \phi$ , for  $\phi > 0$ . If there exist symmetric positive definite matrices  $Q_i \in \mathbb{R}^{n_x \times n_x}$ , matrices  $M_i \in \mathbb{R}^{n_u \times n_y}$ ,  $X \in \mathbb{R}^{n_y \times n_y}$ ,  $Z_i \in \mathbb{R}^{n_w \times n_w}$ , for  $i \in \Omega_N$ , and positive scalars  $\epsilon, \gamma$  satisfying the following optimization:

minimize  $\gamma^2$

subject to (29), (30), (31) and the following conditions:

$$Q_i \geq \phi^2 I \quad (39)$$

$$\begin{bmatrix} Q_i & \star & \star \\ (M_i C_y)_{(l)} & \bar{u}_l^2 & \star \\ C_y Q_i - X C_y & -\epsilon M_i^\top & \epsilon(X + X^\top) \end{bmatrix} \geq 0 \quad (40)$$

$$\begin{bmatrix} Q_i & \star \\ H_{(m)} Q_i & 1 \end{bmatrix} \geq 0 \quad (41)$$

where  $i \in \Omega_N$ ,  $l \in \Omega_{n_u}$ ,  $m \in \Omega_q$ . Then, the SOF controller (21) with the control gains given in (33) solves Problem 1. Moreover, the system constraints  $|\mathbf{u}(t)| \leq \bar{u}$  and  $\mathbf{x}(t) \in \mathcal{D}_x$  are enforced for  $\forall t \geq 0$ .

*Proof.* Multiplying (39) by  $\eta_i(\omega) \geq 0$  and summing up for all  $i \in \Omega_N$ , we obtain  $\sum_{i=1}^N \eta_i(\omega) Q_i \geq \phi^2 I$ , which implies that

$$\mathbf{x}(0)^\top Q(\omega)^{-1} \mathbf{x}(0) \leq \frac{1}{\phi^2} \mathbf{x}(0)^\top \mathbf{x}(0) \leq 1 \quad (42)$$

for  $\forall \mathbf{x}(0) \in \mathbb{R}^{n_x}$  such that  $|\mathbf{x}(0)| \leq \phi$ . This means that condition (39) guarantees  $V(\mathbf{x}(0)) \leq 1$ . Now, multiplying (40) by  $\eta_i(\omega) \geq 0$  and summing up for all  $i \in \Omega_N$  yields

$$\begin{bmatrix} Q(\omega) & \star & \star \\ (M(\omega)C_y)_{(l)} & \bar{u}_l^2 & \star \\ C_y Q(\omega) - X C_y & -\epsilon M(\omega)^\top & \epsilon(X + X^\top) \end{bmatrix} \geq 0 \quad (43)$$

Pre- and postmultiplying (43) with  $\begin{bmatrix} I & 0 & 0 \\ 0 & I & M(\omega)X^{-1} \end{bmatrix}$  and its transpose, we obtain (44) after some simple manipulations.

$$\begin{bmatrix} Q(\omega) & \star \\ (K(\omega)C_y Q(\omega))_{(l)} & \bar{u}_l^2 \end{bmatrix} \geq 0 \Leftrightarrow \begin{bmatrix} Q(\omega)^{-1} & \star \\ (K(\omega)C_y)_{(l)} & \bar{u}_l^2 \end{bmatrix} \geq 0 \quad (44)$$

By Schur complement lemma, this latter is equivalent to

$$\mathbf{x}^\top Q(\omega)^{-1} \mathbf{x} \geq \frac{1}{\bar{u}_l^2} \mathbf{x}^\top (K(\omega)C_y)_{(l)}^\top (K(\omega)C_y)_{(l)} \mathbf{x} \quad (45)$$

for  $\forall \mathbf{x} \in \mathbb{R}^{n_x}$ . Since (see also (42))

$$\mathbf{x}(t)^\top Q(\omega)^{-1} \mathbf{x}(t) \leq \mathbf{x}(0)^\top Q(\omega)^{-1} \mathbf{x}(0) \leq 1, \quad \forall t \geq 0 \quad (46)$$

it follows from (45) that

$$\mathbf{x}^\top (K(\omega)C_y)_{(l)}^\top (K(\omega)C_y)_{(l)} \mathbf{x} \leq \bar{u}_l^2, \quad l \in \Omega_{n_u},$$

which means that  $|\mathbf{u}(t)| \leq \bar{u}$ ,  $\forall t \geq 0$ .

Applying Schur complement lemma to (41), then multiplying the result by  $\eta_i(\omega) \geq 0$  and summing up for all  $i \in \Omega_N$ , we obtain  $Q(\omega)^{-1} \geq H_{(m)}^\top H_{(m)}$ , for  $\forall m \in \Omega_q$ . Combining with (46), this latter condition implies clearly that

$$1 \geq \mathbf{x}^\top Q(\omega)^{-1} \mathbf{x} \geq \mathbf{x}^\top H_{(m)}^\top H_{(m)} \mathbf{x}, \quad \forall m \in \Omega_q,$$

which guarantees that  $\mathbf{x} \in \mathcal{D}_x$ , see [18, Chapter 5]. The rest of the proof follows directly from the result of Theorem 1.  $\square$

**Remark 7.** By a judicious introduction of the scalar  $\epsilon$  and the slack variable  $X$  into the design conditions in Theorems 1 and 2, the complex couplings between Lyapunov matrices, control feedback gains and state-space matrices can be avoided. This enables an LMI-based formulation with a line search over a scalar for SOF control without explicitly requiring any matrix equality constraint and/or matrix rank condition as in most of existing works, see [19] for a recent survey. The proposed SOF control design belongs to the class of  $S$ -variable approach discussed in [32]. Some other notable SOF control results for linear systems based on  $S$ -variable approach can be found in [31], [33], [34] and related references.

**Remark 8.** The design conditions in Theorems 1 and 2 are a set of LMIs with a line search over  $\epsilon$ . The control gains  $K_i$ ,  $i \in \Omega_N$ , can be easily computed with YALMIP toolbox and SDPT3 solver [35] performing a line search for  $\epsilon$  over a logarithmic scale in  $[10^{-6}, 10^6]$ .

**Remark 9.** For multiobjective control design, the proposed control approach offers a possibility to use  $V(\mathbf{x})$  defined in (23) to guarantee the  $\mathcal{H}_2$  control performance as in Theorem 1 and a new Lyapunov function  $\hat{V}(\mathbf{x}) = \mathbf{x}^\top \left( \sum_{i=1}^N \eta_i(\omega) \hat{Q}_i \right)^{-1} \mathbf{x}$ , where  $\hat{Q}_i > 0$ , for  $\forall i \in \Omega_N$ , to enforce the constraints  $|\mathbf{u}(t)| \leq \bar{u}$  and  $\mathbf{x}(t) \in \mathcal{D}_x$ , for  $\forall t \geq 0$ . Although it could help to reduce further the design conservatism, this may lead, however, to additional computational burden to compute the SOF controller (21) with the line search described above. As shown in the next section, Theorem 2 can provide an effective SOF controller for direct tilt control of the SMERA vehicle with a reasonable numerical complexity.

## V. SIMULATION RESULTS AND DISCUSSIONS

The nonlinear model (1) of the SMERA vehicle is used to simulate the performance of the SOF controller (21) designed in Section IV. It is important to note that a validation study of model (1) with experimental data collected from the SMERA vehicle was carried out to identify the vehicle parameters. Moreover, due to industrial confidentiality reasons, all the result figures are slightly scaled so that the vehicle characteristics are not revealed. The following state constraints are considered for the control design:

$$|\theta(t)| \leq 0.35 \text{ [rad]}, \quad |a_{\text{per}}(t)| \leq 1 \text{ [m/s}^2\text{]} \quad (47)$$

Note that the first state constraint aims to prevent the vehicle rollover while cornering, and the second one is directly related to the comfort of passengers. It follows from (7) that

$$a_{\text{per}}(v_x) = \mathcal{G}(v_x)\mathbf{x}_p + G_2 B_\delta \delta,$$

where  $\mathcal{G}(v_x) = G_1(v_x) + G_2 A_p(v_x)$ . Using the variable change of scheduling parameter as described in Section III-D together with the sector nonlinearity approach [27] yields

$$a_{\text{per}}(\omega) = \sum_{i=1}^2 \eta_i(\omega) \mathcal{G}_i \mathbf{x}_p + G_2 B_\delta \delta,$$

where  $\mathcal{G}_1 = \mathcal{G}(\omega_{\min})$  and  $\mathcal{G}_2 = \mathcal{G}(\omega_{\max})$ . Now, the state constraints (47) can be easily put in the form (38) for control design. The control input constraint  $\bar{u} = 40 \text{ [Nm]}$  is the physical limitation of the DTC actuator<sup>2</sup>. Solving the optimization problem in Theorem 2 leads to the following result:

$$\begin{aligned} K_1 &= [3059.4 \quad -46142 \quad -5772.7 \quad 937.16 \quad 31480 \quad 5693.5] \\ K_2 &= [3447.1 \quad -38962 \quad -3848.6 \quad 827.72 \quad 35565 \quad 3864.9] \end{aligned} \quad (48)$$

and  $\gamma = 27.3$ , with  $\epsilon = 0.012$ . The computation time to perform the line search described in Remark 8 is about 197 seconds. Observe that the two control gains corresponding to LPV model (15) are significantly different. This also justifies *a posteriori* the interest of using LPV controller (21) to improve the closed-loop performance since the vehicle speed is time-varying. Solving the same design conditions while imposing  $Q_1 = Q_2 = Q$  (i.e., quadratic approach), we obtain  $\gamma_{\text{quad}} = 34.4 > \gamma$ , with  $\epsilon_{\text{quad}} = 0.003$  and a line search computation time of about 124 seconds. Thus, the quadratic approach leads to more than 20% of degradation in terms of  $\mathcal{H}_2$  performance for this application. This confirms the interest of considering the physical limitations of both vehicle speed and acceleration into the control design to reduce the conservatism, see Remark 6.

### A. Scenario 1: Vehicle Circular Trajectory

This scenario represents a situation for which the SMERA vehicle takes a medium-sized roundabout with a constant speed  $v_x = 6 \text{ [m/s]}$ . As depicted in Fig. 5 (a), the vehicle starts turning at  $t = 2\text{ s}$  and the steering angle  $\delta$  gradually attains its absolute maximal value  $0.22 \text{ [rad]}$  at  $t = 8\text{ s}$ . Then, the vehicle performs a circular trajectory with a constant radius ( $R \approx 19 \text{ [m]}$ ), see Fig. 5 (b). Note that this test scenario is much challenging compared to those tested in [8], [11] with a constant radius about  $500 \text{ [m]}$ . Observe in Fig. 5 (c) that the perceived acceleration  $a_{\text{per}}(t)$  is quite small in the transient phase. In particular, this acceleration is also perfectly regulated during the circular trajectory. Fig. 5 (d) shows that the tilt torque  $M_t$  is within the physical limitations of DTC actuator during the whole test scenario.

Fig. 6 depicts the closed-loop behavior of the vehicle obtained with LPV controller given by Theorem 1. It is stressed that without any guarantee on the control input amplitude, the value of the designed input  $\mathbf{u}(t)$  becomes *excessively* large during roundabout taking, which causes a saturation of DTC actuator as depicted in Figs. 6 (a) and

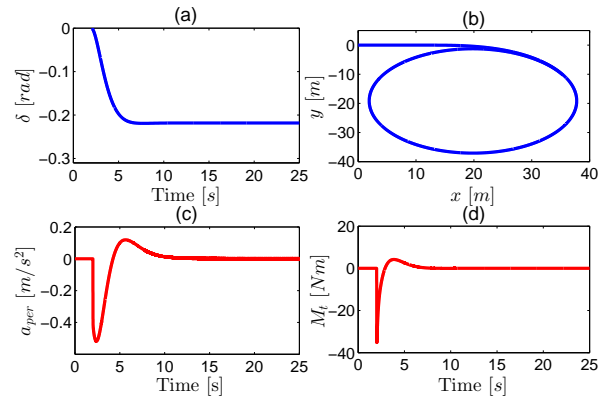


Fig. 5. Scenario 1: Closed-loop behavior of SMERA when actuator limitations are taken into account in the  $\mathcal{H}_2$  control. (a) steering angle; (b) vehicle trajectory; (c) perceived acceleration; (d) tilt torque.

(b), respectively. As a result, the perceived acceleration cannot be regulated in this case, see Fig. 6 (c). Moreover, the vehicle variables tend to be saturated with excessive amplitudes when the vehicle takes the roundabout as shown in Figs. 6 (c), (d), (e) and (f). It is important to note also that a similar closed-loop behavior of the SMERA vehicle is obtained when using the gain-scheduling controller proposed in [6]. This clearly demonstrates the interest of considering the DTC actuator limitations in the  $\mathcal{H}_2$  control design. Furthermore, the gain scheduling technique used in [6] can lead to a tedious and time-consuming design procedure *without* any rigorous guarantee of the closed-loop performance. These facts emphasize the contributions of the proposed control method compared to the existing literature.

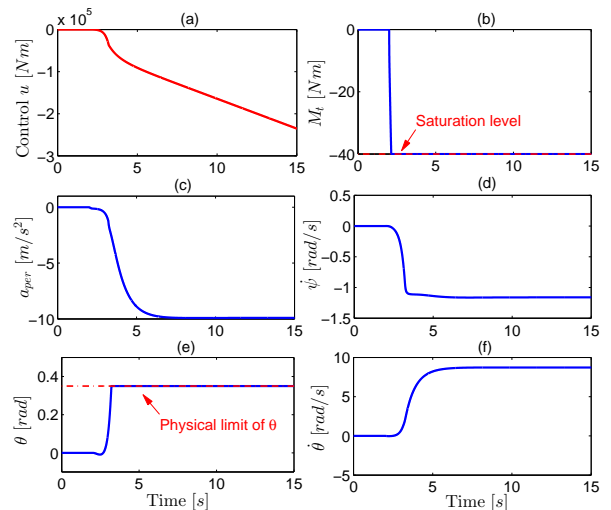


Fig. 6. Scenario 1: Closed-loop behavior of SMERA when actuator limitations are *not* taken into account in the  $\mathcal{H}_2$  control. (a) control input; (b) tilt torque; (c) perceived acceleration; (d) yaw rate; (e) tilt angle; (f) tilt rate.

### B. Scenario 2: Bend-taking with Time-Varying Speed

This scenario represents a situation for which the SMERA vehicle takes two successive bends with a highly *time-varying* vehicle speed, see Figs. 7 (a) and (b). To demonstrate the interest of taking into account the time-varying nature of the vehicle speed in the DTC control design, the performance comparison between two following SOF controllers is considered:

- **LPV controller** whose feedback gains are given in (48).
- **Linear time-invariant (LTI) controller** whose linear feedback gain is synthesized under similar design conditions as for the above LPV controller with a *constant* speed  $v_x = 8 \text{ [m/s]}$ .

The comparison results are depicted in Figs. 7 (c), (d), (e), (f), (g) and (h). It can be observed that the LPV controller provides a clear

<sup>2</sup>For real-time implementation, the *hard* constraint on the physical limitation of the tilt torque is guaranteed by the “Saturation” block in Simulink.

performance improvement compared to the LTI one, especially in terms of acceleration regulation and transient behavior of the tilt torque  $M_t$ . Fig. 7 (c) also shows that the perceived acceleration is well regulated by the LPV controller with an acceptable maximal amplitude about  $0.7 [m/s^2]$  during transient phases. The tilt torque  $M_t$  remains within its saturation limits for both SOF controllers during the whole test as shown in Fig. 7 (d). Note that the considered test scenario is much more challenging than those used in other DTC control contexts of NTVs [6], [8], [11], [21], *i.e.*, driving scenarios with low and/or constant vehicle speed and very large bends. It is important to note also that for this challenging scenario, the gain-scheduling controller proposed in [6] also provides an *unstable* closed-loop behavior, which is not shown here for brevity.

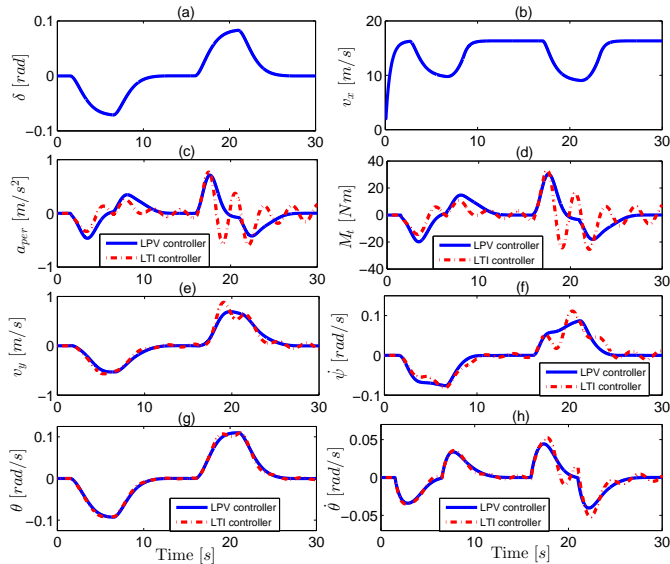


Fig. 7. Scenario 2: Control performance comparison. (a) steering angle; (b) vehicle speed; (c) perceived acceleration; (d) tilt torque; (e) lateral speed; (f) yaw rate; (g) tilt angle; (h) tilt rate.

## VI. CONCLUDING REMARKS

This paper proposes a new LPV control method for automatic DTC of NTVs. For real-time control implementation, only common sensors available on commercial vehicles are required and the robust SOF controller is of the simplest structure. The proposed DTC method is formulated as an LMI-based optimization in multiobjective setting. Based on the use of a PDLF, the information on both speed and acceleration limitations is incorporated into the design of robust DTC controllers to reduce the conservatism. The effectiveness of the proposed method is clearly demonstrated with realistic driving scenarios. Our future works focus on the shared control between a human driver and a STC system (see for instance [24]) in the presence of DTC control actions. Moreover, experimental validations of the proposed DTC method in real-world driving conditions should be also investigated.

## REFERENCES

- [1] J. C. Chiou and C. L. Chen, "Modeling and verification of a diamond-shape narrow-tilting vehicle," *IEEE/ASME Trans. Mechatron.*, vol. 13, no. 6, pp. 678–691, 2008.
- [2] J. Berote, J. Darling, and A. Plummer, "Development of a tilt control method for a narrow-track three-wheeled vehicle," *Proc. Inst. Mech. Eng. Pt. D J. Automobile Eng.*, vol. 226, no. 1, pp. 48–69, 2012.
- [3] S. Kidane, R. Rajamani, L. Alexander, P. J. Starr, and M. Donath, "Development and experimental evaluation of a tilt stability control system for narrow commuter vehicles," *IEEE Trans. Control Syst. Technol.*, vol. 18, no. 6, pp. 1266–1279, 2010.
- [4] M. Ataci, A. Khajepour, and S. Jeon, "Reconfigurable integrated stability control for four- and three-wheeled urban vehicles with flexible combinations of actuation systems," *IEEE/ASME Trans. Mechatron.*, vol. 23, no. 5, pp. 2031–2041, 2018.
- [5] J. Sindha, B. Chakraborty, and D. Chakravarty, "Automatic stability control of three-wheeler vehicles—recent developments and concerns towards a sustainable technology," *Proc. Inst. Mech. Eng. Pt. D J. Automobile Eng.*, vol. 232, no. 3, pp. 418–434, 2018.
- [6] L. Mourad, F. Claveau, and P. Chevrel, "Direct and steering tilt robust control of narrow vehicles," *IEEE Trans. Intell. Transp. Syst.*, vol. 15, no. 3, pp. 1206–1215, 2014.
- [7] R. Rajamani, J. Gohl, L. Alexander, and P. Starr, "Dynamics of narrow tilting vehicles," *Math. Comput. Model. Dyn. Syst.*, vol. 9, no. 2, pp. 209–231, 2003.
- [8] D. Piyabongkarn, T. Keviczky, and R. Rajamani, "Active direct tilt control for stability enhancement of a narrow commuter vehicle," *Int. J. Automot. Technol.*, vol. 5, no. 2, pp. 77–88, 2004.
- [9] S. Maakaroun, W. Khalil, M. Gautier, and P. Chevrel, "Modeling and simulating a narrow tilting car using robotics formalism," *IEEE Trans. Intell. Transp. Syst.*, vol. 15, no. 3, pp. 1026–1038, 2014.
- [10] M. Corno, G. Panzani, and S. M. Savaresi, "Single-track vehicle dynamics control: state of the art and perspective," *IEEE/ASME Trans. Mechatron.*, vol. 20, no. 4, pp. 1521–1532, 2015.
- [11] R. Hibbard and D. Karnopp, "Twenty first century transportation system solutions—a new type of small, relatively tall and narrow active tilting commuter vehicle," *Veh. Syst. Dyn.*, vol. 25, no. 5, pp. 321–347, 1996.
- [12] M. Chatterjee, M. Kale, and B. Chaudhari, "A dynamic stability control for electric narrow tilting three wheeled vehicle using integrated multivariable controller," *Transp. Res. D Transp. Environ.*, 2017.
- [13] N. Roqueiro, M. G. De Faria, and E. F. Colet, "Sliding mode controller and flatness based set-point generator for a three wheeled narrow vehicle," *IFAC Proc. Vol.*, vol. 44, no. 1, pp. 11925–11930, 2011.
- [14] J. M. Snider, "Automatic steering methods for autonomous automobile path tracking," Robotics Institute, Carnegie Mellon University, Pittsburgh, USA, Tech. Rep. CMU-RI-TR-09-08, 2009.
- [15] J. Mohammadpour and C. Scherer, *Control of Linear Parameter Varying Systems with Applications*. Springer Science & Business Media, 2012.
- [16] O. Sename, P. Gaspar, and J. Bokor, *Robust Control and Linear Parameter Varying Approaches: Application to Vehicle Dynamics*. Springer, 2013.
- [17] C. Briat, *Linear Parameter-Varying and Time-Delay Systems: Analysis, Observation, Filtering & Control*. Springer, 2014.
- [18] S. Boyd, L. El Ghaoui, E. Feron, and V. Balakrishnan, *Linear Matrix Inequalities in System and Control Theory*. Philadelphia: SIAM, 1994.
- [19] M. S. Sadabadi and D. Peaucelle, "From static output feedback to structured robust static output feedback: A survey," *Ann. Rev. Control*, vol. 42, pp. 11–26, 2016.
- [20] C. Tang, L. He, and A. Khajepour, "Design and analysis of an integrated suspension tilting mechanism for narrow urban vehicles," *Mech. Mach. Theory*, vol. 120, pp. 225–238, 2018.
- [21] H. Furuichi, J. Huang, T. Fukuda, and T. Matsuno, "Switching dynamic modeling and stability analysis of three-wheeled narrow tilting vehicle," *IEEE/ASME Trans. Mechatron.*, vol. 19, no. 4, pp. 1309–1322, 2014.
- [22] S. Fuchshumer, K. Schlacher, and T. Rittenschober, "Nonlinear vehicle dynamics control - A flatness based approach," in *Proc. 44th IEEE Conf. Dec. Control, Eur. Control Conf.*, 2005, pp. 6492–6497.
- [23] H. Pacejka, *Tire and Vehicle Dynamics*. Elsevier, 2005.
- [24] A.-T. Nguyen, C. Sentouh, and J.-C. Popieul, "Sensor reduction for driver-automation shared steering control via an adaptive authority allocation strategy," *IEEE/ASME Trans. Mechatron.*, vol. 23, no. 1, pp. 5–16, 2018.
- [25] P. Lundström, S. Skogestad, and Z.-Q. Wang, "Performance weight selection for  $\mathcal{H}_\infty$  and  $\mu$ -control methods," *Trans. Inst. Meas. Control*, vol. 13, no. 5, pp. 241–252, 1991.
- [26] A.-T. Nguyen, C. Sentouh, and J.-C. Popieul, "Driver-automation cooperative approach for shared steering control under multiple system constraints: Design and experiments," *IEEE Trans. Ind. Electron.*, vol. 64, no. 5, pp. 3819–3830, 2017.
- [27] K. Tanaka and H. Wang, *Fuzzy Control Systems Design and Analysis: a Linear Matrix Inequality Approach*. NY: Wiley-Interscience, 2004.
- [28] C. de Souza and A. Trofino, "Gain-scheduled  $\mathcal{H}_2$  controller synthesis for linear parameter varying systems via parameter-dependent Lyapunov functions," *Int. J. Robust Nonlin. Control*, vol. 16, no. 5, pp. 43–57, 2006.
- [29] A. Sala and Arino, "Asymptotically necessary and sufficient conditions for stability and performance in fuzzy control: Applications of Polya's theorem," *Fuzzy Sets Syst.*, vol. 158, no. 24, pp. 2671–2686, 2007.
- [30] H. Tuan, P. Apkarian, T. Narikiyo, and Y. Yamamoto, "Parameterized linear matrix inequality techniques in fuzzy control system design," *IEEE Trans. Fuzzy Syst.*, vol. 9, no. 2, pp. 324–332, 2001.
- [31] A.-T. Nguyen, P. Chevrel, and F. Claveau, "Gain-scheduled static output feedback control for saturated LPV systems with bounded parameter variations," *Automatica*, pp. 420–424, 2018.
- [32] Y. Ebihara, D. Peaucelle, and D. Arzelier, *S-Variable Approach to LMI-Based Robust Control*. Springer, 2015.
- [33] C. Agulhari, R. Oliveira, and P. Peres, "LMI relaxations for reduced-order robust  $\mathcal{H}_\infty$  control of continuous-time uncertain linear systems," *IEEE Trans. Autom. Control*, vol. 57, no. 6, pp. 1532–1537, 2012.
- [34] J. Dong and G.-H. Yang, "Robust static output feedback control synthesis for linear continuous systems with polytopic uncertainties," *Automatica*, vol. 49, no. 6, pp. 1821–1829, 2013.
- [35] J. Löfberg, "Yalmip: A toolbox for modeling and optimization in Matlab," in *IEEE Int. Symp. Comput. Aided Control Syst. Des.*, Taipei, 2004, pp. 284–289.